Plasmonics
DOI 10.1007/s11468-015-0042-z

Unidirectional All-Optical Absorption Switch Based on Optical Tamm State in Nonlinear Plasmonic Waveguide

Miaosheng Fang[1,2] · **Fenghua Shi**[1,2] · **Yihang Chen**[1,2]

Received: 9 May 2015 / Accepted: 26 July 2015

Abstract We demonstrate that unidirectional absorption can be achieved and efficiently tuned in an asymmetrical and nonlinear metal-dielectric-metal plasmonic waveguide by inserting a one-dimensional photonic crystal and a metal layer into the waveguide core. We show that optical Tamm state is excited when the surface impedance of the photonic crystal and that of the metallic layer match with each other. Owing to the strong field confinement induced by the optical Tamm state, high absorption of the surface plasmon can be achieved in the proposed waveguide. The geometric asymmetry of the considered system makes its absorption performance quite different for different incident directions, which is useful for the design of unidirectional plasmonic absorber. Furthermore, Fano resonance, originating from the quantum interference between the optical Tamm state and the traveling waveguide mode, occurs and can be tuned through the nonlinear optical effect. Based on the tunable Fano asymmetric line shape of the considered system, absorption contrast ratio up to 43.5 dB is achieved by varying the intensity of the pumping light, which can be used for all-optical Fano absorption switching. Our results may find potential applications in integrated optical circuits and photodetection.

Keywords Surface plasmon · Optical Tamm state · Fano resonance · Nonlinear optics

Introduction

Surface plasmon polaritons (SPPs) are known as surface waves propagating along the interface of metal and dielectric owing to the interaction between the free electrons in metal and electromagnetic field in dielectric, and attenuating exponentially in the direction perpendicular to the interface [1, 2]. SPPs have been considered as one of the most promising energy and information carries to overcome the diffraction limit of light and manipulate light in subwavelength nanoscale structures [1]. Metal-dielectric-metal (MDM) plasmonic waveguides have attracted considerable attention in recent years because of their abilities in deep-subwavelength confinement of optical fields and their relatively low fabrication cost [3, 4]. Various kinds of plasmonic devices containing MDM waveguide, such as all-optical switches [5], splitters [6], filters [7], plasmonic diode [8], Mach–Zehnder interferometers [9], and Bragg reflectors [10], have been proposed and investigated.

As an important kind of optical devices, electromagnetic absorbers have found applications in diverse fields, such as photodetection [11–13], imaging [14], solar energy conversion [15], and thermal emission [16]. A number of nanostructures such as carbon nanotube films [17], dielectric matrix embedded with metal particles [18], dielectric diffraction gratings [19], resonant-ring-based metamaterial [20], plasmonic nanoantennas [21], metal-dielectric-metal elliptical nanodisk arrays [22], metal-semiconductor gratings [23], core-shell metamaterials [24], and graphene layers [25] were proposed for achieving high absorption.

Miaosheng Fang and Fenghua Shi contributed equally to this work.

✉ Yihang Chen
yhchen@scnu.edu.cn

[1] Guangdong Provincial Key Laboratory of Quantum Engineering and Quantum Materials, School of Physics and Telecommunication Engineering, South China Normal University, Guangzhou 510006, China

[2] Guangdong Provincial Engineering Research Center for Optoelectronic Instrument, Guangzhou 510006, China

Published online: 07 August 2015

Recently, optical Tamm state (OTS), corresponding to a narrow resonance mode with electromagnetic field localized at the interface inside a photonic crystal (PhC)–metal [26] or a PhC–PhC heterostructure [27], has been applied to polariton lasers [28], absorption enhancement [29], enhancement of Kerr nonlinearity [30], optical switch [31], and optical sensor [32]. It would be interesting to design plasmonic absorption devices or nonlinear plasmonic devices by using the field confinement feature of the OTS. Furthermore, the narrow resonance profile of the OTS may also be used for the excitation of a classical quantum phenomenon, Fano resonance, which originates from the interference of a narrow discrete resonance with a broad spectral line or continuum [33]. In contrast to a Lorentzian resonance, the Fano resonance exhibits a distinctly asymmetric lineshape which can be tuned by the nonlinear effect [34].

In this paper, we propose a novel design of unidirectional all-optical absorption switch using a nonlinear MDM waveguide with OTS. A one-dimensional PhC and a metal layer are placed together inside the waveguide core to excite the OTS. We demonstrate that a surface-impedance-match condition can be used to determine whether and where the OTS occurs. Due to the interaction between the OTS and the traveling waveguide mode, nonlinear Fano resonance is observed under the irradiation of a pumping light. Using the tunable Fano asymmetric lineshape, unidirectional all-optical absorption switch with ultrahigh absorption contrast ratio is realized. Finite difference time domain (FDTD) method and transfer matrix method (TMM) are used to demonstrate our results.

The Model and Simulation Methods

The considered plasmonic waveguide is shown in Fig. 1a, where a one-dimensional PhC and a metallic layer are inserted in the core of a MDM waveguide. Dielectric materials A and B with the lengths of L_A and L_B are stacked alternately to construct the PhC. In the considered system, Al_2O_3 and GaAs are chosen as dielectric A and B, respectively. Al_2O_3 has low dispersion and its refractive index is set as n_A=1.7 [35]. GaAs is a Kerr-type nonlinear material. The linear part of its refractive index n_B^L changes from 3.68 to 3.38 as the wavelength varies from 800 to 1459 nm [35]. The metal is selected as silver, which has a complex relative permittivity characterized by a well-known Drude model $\varepsilon_m(\omega)=\varepsilon_\infty-\omega_p^2/[\omega(\omega+i\gamma)]$. Here, ω is the angular frequency of incident light, ε_∞ is the dielectric constant at the infinite frequency, and γ and ω_p are the electron collision frequency and bulk plasma frequency, respectively. In the following simulations, the parameters for silver are set as ε_∞=3.7, ω_p=9.1 eV and γ=0.018 eV [36], the number of the periods of the PhC is fixed as 4, and the width of the waveguide core w is fixed as 70 nm.

Suppose that a transversal-magnetic (TM) SPP mode is excited and propagates along the waveguide core, as shown in Fig. 1a. The dispersion relation of the fundamental TM mode in MDM structure can be written as [37]

$$\varepsilon_m k_d \tanh\left(-\frac{ik_d}{2}w\right)+\varepsilon_d k_m=0, \tag{1}$$

where w is the width of dielectric layer. ε_d (d=A or B) and ε_m represent the permittivities of dielectric and metal. k_d and k_m are transverse propagation constants in dielectric and metal, respectively. They satisfy

$$k_m^2=\varepsilon_m k_0^2-\beta^2,\quad k_d^2=\varepsilon_d k_0^2-\beta^2, \tag{2}$$

where β is the propagation constant of the SPP and $k_0=2\pi/\lambda_0$ represents the wave number of light in free space. The effective index of the MDM plasmonic waveguide can be obtained from

$$n_{\text{eff}}=\beta/k_0. \tag{3}$$

The effective indices of the MDM waveguide inserted with the Al_2O_3 or GaAs layer can be calculated from Eqs. 1–3 and the wavelength dependence of the effective indices are shown in Fig. 1b, c. It can be seen that the effective indices corresponding to the Al_2O_3 layer and the GaAs layer are quite different, while they both show relatively weak dependence on the wavelength at longer wavelength region. The imaginary parts of n_{eff}, as shown in Fig. 1c, represent the losses of the SPP and determine the propagation length of the SPP wave.

Both finite difference time domain (FDTD) method [38] and transfer matrix method (TMM) are used to investigate the properties of the considered system. For the TMM, the optical properties can be investigated via the product of multiple transfer matrices. In this case, each section of the MDM waveguide with a specific filling dielectric is treated as a layer of medium with a specific effective index. The electric field at position x and $x+\Delta x$ can be related via a transfer matrix

$$\begin{bmatrix}\cos(k\Delta x) & -i/q\sin(k\Delta x)\\ -iq\sin(k\Delta x) & \cos(k\Delta x)\end{bmatrix}, \tag{4}$$

where $k=\omega n_{\text{eff}}$, $q=n_{\text{eff}}$. The transfer matrix for the Ag layer can be written as

$$\begin{bmatrix}\cos(k_mL_m) & -i/q_m\sin(k_mL_m)\\ -iq_m\sin(k_mL_m) & \cos(k_mL_m)\end{bmatrix}, \tag{5}$$

where $k_m=\omega\sqrt{\varepsilon_m}$, $q_m=\sqrt{\varepsilon_m}$, and L_m is the length of the Ag layer. The matrix connecting the incident end and the exit end, i.e., the characteristic matrix for the whole structure, can be obtained by multiplying the characteristic matrix for each section in waveguide. Assuming that the characteristic matrix for the

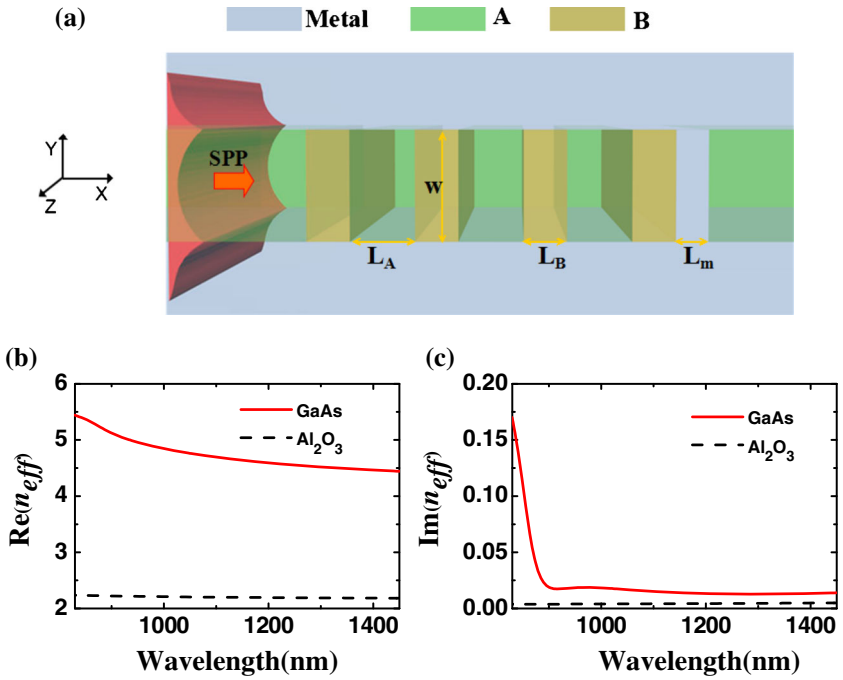

Fig. 1 **a** Schematic diagram of the proposed plasmonic waveguide. A PhC composed of dielectric layer *A* (Al_2O_3) and *B* (GaAs) is placed together with a metallic layer inside the waveguide core. **b** Real and **c** imaginary parts of the effective refractive indexes for the SPP inside the layer *A* and *B*, respectively

considered waveguide is *X*, the transmittance and the reflectance can be written as [39]

$$T = \left| \frac{2}{X_{11} + X_{22} + X_{21} + X_{12}} \right|^2, \tag{6}$$

$$R = \left| \frac{X_{11} + X_{12} - X_{21} - X_{22}}{X_{11} + X_{12} + X_{22} + X_{21}} \right|^2, \tag{7}$$

where X_{ij} (i,j= 1,2) is the elements of *X*. The surface impedance *Z* of the plasmonic waveguide is

$$Z = \frac{X_{21} + X_{22}}{X_{11} + X_{12}}. \tag{8}$$

Design of the OTS-Based Unidirectional Absorption in MDM Plasmonic Waveguide

Figure 2 shows the transmittance and reflectance as a function of wavelength for the MDM waveguide where only an Ag layer (with L_m=70 nm) or a PhC $(AB)^4$ (with L_A=84 nm and L_B=68 nm) is placed inside the waveguide core. One can see that both the waveguide structures exhibit high reflection at the wavelength range from 950 to 1350 nm. The simulation results from the FDTD method and those from the TMM agree well with each other.

OTS is known as a confined electromagnetic mode which exists at the boundary between two medium with high reflection. OTS emerges when the resonant condition of a zero-length cavity is satisfied [40]. Here, r_{PhC}(r_{Ag}) and Z_{PhC}(Z_{Ag}) are used to denote the reflection coefficient and the impedance of the MDM waveguide where a PhC (silver layer) is inserted inside the waveguide core. When the absorption loss is considered, the impedance is complex. Then, we have

$$r_{PhC} = \frac{Z_0 - Z_{PhC}}{Z_0 + Z_{PhC}} = \frac{Z_0 - (Z_{PhC}' + iZ_{PhC}'')}{Z_0 + (Z_{PhC}' + iZ_{PhC}'')} = \frac{\left[\left(Z_0 + Z_{PhC}''^2 - Z_{PhC}'^2\right) - 2iZ_{PhC}''\right]}{(Z_0 + Z_{Ph}')^2 + Z_{PhC}''^2} \tag{9}$$

$$r_{Ag} = \frac{Z_0 - Z_{Ag}}{Z_0 + Z_{Ag}} = \frac{Z_0 - (Z_{Ag}' + iZ_{Ag}'')}{Z_0 + (Z_{Ag}' + iZ_{Ag}'')} = \frac{\left[\left(Z_0 + Z_{Ag}''^2 - Z_{Ag}'^2\right) - 2iZ_{Ag}''\right]}{(Z_0 + Z_{Ag}')^2 + Z_{Ag}''^2}, \tag{10}$$

where Z_0 is the impedance of the MDM waveguide with an air core.

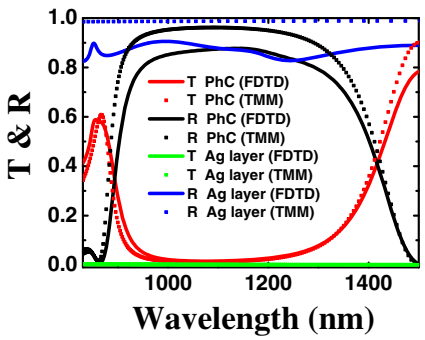

Fig. 2 Reflection (*R*) and transmission (*T*) spectra for the MDM waveguide inserted with a PhC $(AB)^4$ with L_A=94 nm and L_B=68 nm or an Ag layer with L_m= 70 nm

The OTS corresponding to a zero reflection can be observed when the conditions $|r_{PhC}|=|r_{Ag}|$ and $\varphi(r_{PhC})=-\varphi(r_{Ag})$ are satisfied simultaneously. Combining with Eqs. 9 and 10, such conditions can be written as $Z_{PhC}'=Z_{Ag}'$ and $Z_{PhC}''=-Z_{Ag}''$, i.e., $|Z_T|=|Z_{PhC}'-Z_{Ag}'|+|Z_{PhC}''+Z_{Ag}''|=0$. If the condition $|Z_T|=0$ cannot be satisfied, OTS will appear at the frequency where $|Z_T|$ is minimum [41]. Therefore, from the variation of $|Z_T|$, we can determine where the OTS exists. Figure 3a shows the dependence of $|Z_T|$ on wavelength for the waveguide with L_A=94 nm, L_B=68 nm, and L_m=70 nm. It can be seen from Fig. 3a that $|Z_T|$ reaches a minimum value at 1262 nm. Consequently, an OTS should emerge at the corresponding wavelength.

In low-loss cases, the OTS can be detected by measuring the transmittance because it corresponds to a narrow transmission peak [42]. However, for the considered plasmonic waveguide, the strong field confinement induced by the OTS will give rise to large absorption loss inside the metallic structure. Hence, an absorption peak is anticipated to emerge at the wavelength of the OTS. Figure 3b shows the absorptance as a function of wavelength for the MDM waveguide inserted with the heterostucture $(AB)^4$-Ag. It can be seen that an absorption peak appears in both TMM (at 1262 nm) and FDTD (at 1245 nm) simulations for the forward (along $+x$ direction) incident wave. The absorptance of the peak is over 0.985. The difference between the FDTD and TMM results is mainly attributed to the difference between the values of ε_m obtained from the ideal Drude model (in the TMM simulations) and those obtained from the measured data (in the FDTD simulations). The wavelength of the perfect absorption peak is the same as that corresponding to the minimum value of $|Z_T|$. Therefore, the surface-impedance-match condition can be used to predict where the OTS-based absorption peak appears. On the other hand, for the backward (along $-x$ direction) incident wave, the absorptance remains very low, although there is still a low absorption peak (absorptance is lower than 0.09) at the wavelength of the OTS, as shown in Fig. 3b.

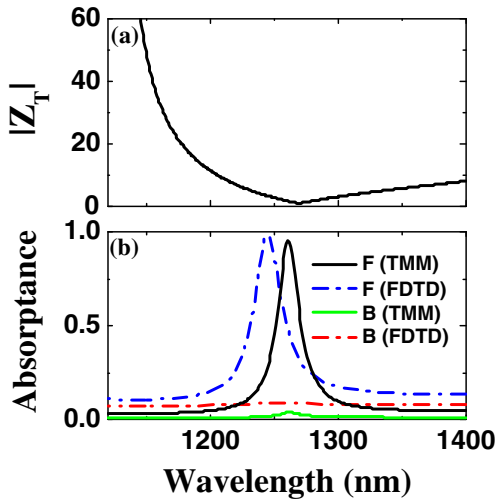

Fig. 3 **a** Dependence of $|Z_T|$ on wavelength for the MDM plasmonic waveguide. **b** Absorptance as a function of wavelength for the MDM waveguide embedded with the $(AB)^4$-Ag heterostructure. *F* and *B* represent the forward (along $+x$ direction) and backward (along $-x$ direction) incident light, respectively. The geometric parameters are L_A=94 nm, L_B=68 nm, and L_m=70 nm

To understand the phenomenon of the unidirectional absorption, we continue to investigate the properties of the surface impedance of the plasmonic waveguide. Here, we use Z_A to denote the surface impedance of the MDM waveguide and Z_{hetero} to denote the MDM waveguide inserted with the heterostructure $(AB)^4$-Ag. We then define $|Z_C^{(F)}|=|Z_{hetero}^{(F)}-Z_A^{(F)}|$ and $|Z_C^{(B)}|=|Z_{hetero}^{(B)}-Z_A^{(B)}|$, where *F* and *B* represent the forward and backward incidence, respectively. Figure 4 shows the values of $|Z_C^{(F)}|$ and $|Z_C^{(B)}|$ as a function of the wavelength. For the forward incident wave, $|Z_C^{(F)}|$ drops to a minimum at 1262 nm, which means that a good impedance matching and consequently a weak reflection occur. In this case, most of the energy will be absorbed due to the excitation of the OTS. For the backward incident wave, it can be seen from Fig. 4b that $|Z_C^{(B)}|$ cannot reach a relatively small value in the vicinity of the OTS's wavelength; thus, strong reflection occurs due to the impedance mismatch. Therefore, the absorption corresponding to the OTS becomes much weaker. The full wavelength at half maximum (FWHM) of the absorption peak is about 28 nm, which may find applications in sensing and imaging.

For further verification of the OTS-based absorption, we simulate the magnetic field distributions using FDTD method with the spatial sizes $\Delta x=\Delta y=1$ nm. Figure 5a, b shows the spatial distributions of H_z for the forward incident wave at 1030 and 1245 nm, respectively. For the case at 1030 nm, strong reflection is observed because the wavelength locates inside the photonic band gap of the PhC; thus, the absorption of the waveguide is very low. For the case at 1245 nm, the field can propagate through the PhC-Ag heterostructure due to

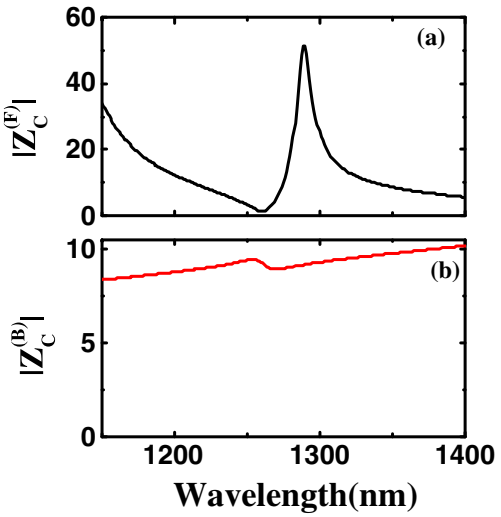

Fig. 4 Dependence of **a** $|Z_C^{(F)}|$ and **b** $|Z_C^{(B)}|$ on wavelength for the considered MDM waveguide embedded with the heterostructure $(AB)^4$-Ag

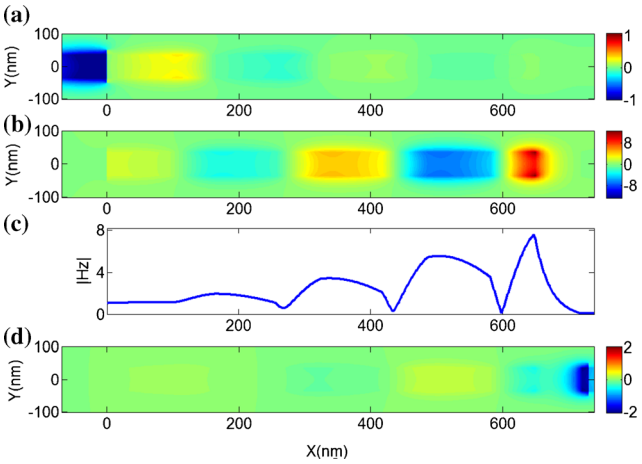

Fig. 5 Distributions of H_z inside the proposed plasmonic waveguide for the forward incident wave at **a** 1030 nm and **b** 1245 nm, respectively. **c** Amplitude of magnetic field $|H_z|$ vs x coordinate (y=0) at the wavelength of 1245 nm. The interface between $(AB)^4$ and the Ag layer inside the heterostructure is at x=648 nm. **d** Distribution of Hz for the backward incident wave at 1245 nm

the excitation of the OTS. Figure 5c shows the dependence of $|H_z|$ on x coordinate at 1245 nm. It can be seen that strongest field localization appears at x=648 nm, the position of the interface between the PhC $(AB)^4$ and the Ag layer, which agrees with the characteristic of the OTS. Such strong field localization leads to the high absorption inside the considered plasmonic waveguide. For comparison, we also calculate the distribution of H_z for the backward incident wave at 1245 nm, as shown in Fig. 5d. It can be seen that strong reflection occurs because of the impedance mismatch, as mentioned before.

Dependence of the Unidirectional Absorption Peak on the Geometric Parameters

Next, we study the dependence of the OTS-based absorption on the geometric parameters of the considered plasmonic

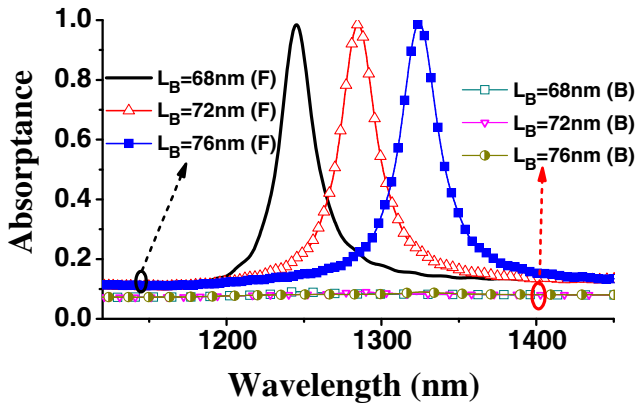

Fig. 6 Absorptance vs wavelength under different values of L_B for the proposed waveguide inserted with the heterostructure $(AB)^4$-Ag. The other geometric parameters are L_A=94 nm and L_m=70 nm. F and B represent the forward and backward incident light, respectively

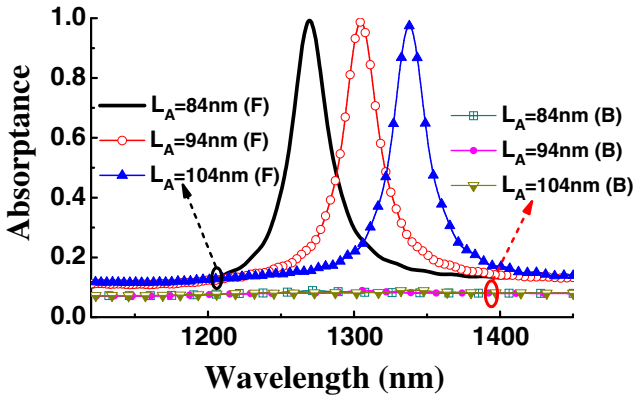

Fig. 7 Absorptance vs wavelength under different values of L_A for the proposed waveguide with L_B=74 nm and L_m=70 nm

waveguide. In Fig. 6, we plot the absorptance versus the wavelength under different values of L_B for the proposed plasmonic waveguide with L_A=94 nm and L_m=70 nm. As shown in Fig. 6, the absorption peak shifts to longer wavelength (from 1245 to 1324 nm) as the increase of L_B (from 68 to 76 nm) for the forward incident wave, while the absorptance remains quite low under backward incidence. The shift of the absorption peak results from the changes of the wavelength where the surface-impedance-match is satisfied. Moreover, we also investigate the dependence of the OTS-based absorption peak on L_A for the waveguide with L_B=74 nm and L_m=70 nm, as shown in Fig. 7. It can be seen that the unidirectional absorption peak shifts from 1270 to 1338 nm as the value of L_A changes from 84 to 104 nm. Therefore, the OTS-based unidirectional absorption peak can be tuned to the position as desired by varying the geometric parameters.

Unidirectional All-Optical Absorption Switch Based on Nonlinear Fano Resonance

Since Kerr-type nonlinear material GaAs was introduced into the considered plasmonic system, it is expected that the

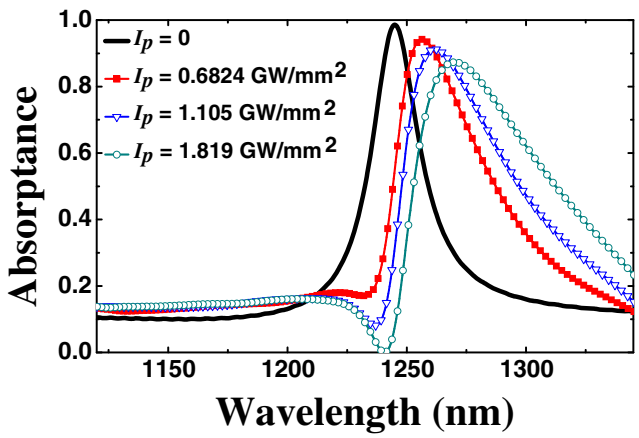

Fig. 8 Absorption spectra at different intensity of the pumping beam under forward incidence. The geometric parameters of the plasmonic waveguide are L_A=94 nm, L_B=68 nm, and L_m=70 nm

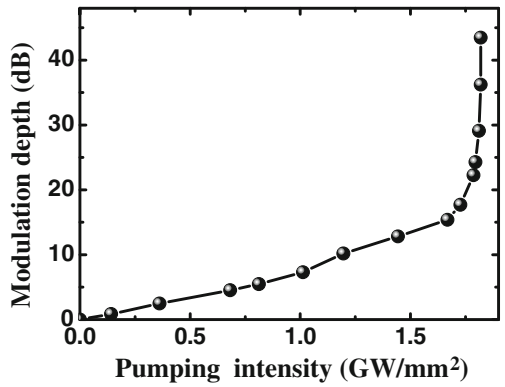

Fig. 9 Modulation depth as a function of the pumping intensity I_p under forward incidence of the signal wave at 1241 nm

absorption properties will be influenced by the nonlinear effect. The dielectric function of GaAs with cubic nonlinearity is

$$\varepsilon_B = \varepsilon_B^L + \chi^{(3)}|E|^2, \tag{9}$$

where ε_B^L and $\chi^{(3)}$ are the linear permittivity and the third-order optical nonlinear susceptibility, respectively. |E| is the intensity of the electric field. In our simulations, we choose $\chi^{(3)}=1\times10^{-10}$ esu [43]. It was reported that strong optical nonlinearity can be observed in metal colloids because of the surface plasma resonance [44]. However, for our considered structure, the nonlinearity of the silver layer is much weaker than that of GaAs [43], and the electric field inside the GaAs layers is much stronger than that inside the Ag layer. Therefore, the nonlinear effect of silver excited by the pumping wave is very weak and will be neglected in the following simulations. To excite the nonlinear response, a pumping beam with the wavelength of 1225 nm is introduced into the waveguide. Figure 8 shows the absorption spectra at different intensity of the pump beam under forward incidence. The geometric parameters of the plasmonic waveguide are L_A= 94 nm, L_B=68 nm, and L_m=70 nm. It can be anticipated that the increase of the pumping beam intensity I_p will lead to the increase of the refractive index of GaAs, which results in the redshift of the absorption peak. As shown in Fig. 8, the absorption peak shifts from 1245 to 1270 nm as I_p increases from 0 (absence of the pumping light) to 1.819 GW/mm^2.

Moreover, it can be seen from Fig. 8 that the absorption spectra exhibit asymmetric line shape, the characteristic feature of the Fano resonance, when the pumping light is strong enough. The Fano effect becomes more and more pronounced as the pumping power increases. Such a nonlinear Fano resonance arises when the coherent interference occurs between two competing optical pathways [45]. One corresponds to a discrete state, i.e., the OTS, and the other corresponds to a continuum of energy states, i.e., the traveling modes of the plasmonic waveguide. As shown in Fig. 8, the Fano asymmetric line shape has an absorption dip, resulting from the destructive interference, and an absorption peak, resulting from the constructive interference. When the mode amplitudes corresponding to the continuum and the discrete states are of the same magnitude, the interference effect is strong and pronounced asymmetric profile can be observed [34, 45]. Changing the pumping power is a convenient way to tune the relative strength of the two competing pathways, leading to the variations of the asymmetric line shape of the absorption spectra. The "on"–"off" switching of the Fano asymmetric lineshape can be used for the design of all-optical absorption switch.

Here, we define the modulation depth of the absorption switch as $M_A = 10\log_{10}(A_0/A_I)$, where A_0 is the absorptance when the pump light is off and A_I is the absorptance when the pump light is on. Figure 9 shows the modulation depth as a function of pumping intensity I_p for our considered system under forward incidence of the signal wave at 1241 nm. It is noted that the modulation depth increases with the increasing I_p. Ultrahigh modulation depth of 43.5 dB can be achieved. Thus, these results provide us an efficient way to design tunable ultracompact absorption-based devices.

Conclusions

We have designed a unidirectional all-optical OTS-based absorption switch by using a nonlinear MDM plasmonic waveguide where a PhC–Ag heterostructure was placed inside the waveguide core. OTS was excited at the interface of the heterostructure, which agrees with the prediction of the surface-impedance-match condition. Strong absorption of the considered waveguide can be achieved due to the field confinement of the OTS. The absorption performance of the considered system is quite different for different incident directions, which is attributed to the geometric asymmetry of the waveguide structure. Fano-type asymmetric lineshape based on the interaction of the OTS and the traveling plasmonic modes was observed and can be turned on and off through the nonlinear optical effect. Ultrahigh modulation depth 43.5 dB of the absorption is realized by using the tunable Fano resonance in the proposed system. The presented design with compact dimensions may find applications in integrated optical circuits, sensors, and photodetection.

Acknowledgments This work was supported by National Natural Science Foundation of China (Grant No. 11274126). Y.H. Chen acknowledges financial support from Program for Guangdong Provincial Excellent Young Teacher.

References

1. Barnes WL, Dereux A, Ebbesen TW (2003) Surface plasmon subwavelength optics. Nature 424:824–830
2. Zhang Q, Huang XG, Lin XS, Tao J, Jin XP (2009) A subwavelength coupler-type MIM optical filter. Opt Express 17:7549–7554

3. Neutens P, Dorpe PV, Vlaminck ID, Lagae L, Borghs G (2009) Electrical detection of confined gap plasmons in metal-insulator-metal waveguides. Nat Photonics 3:283–286
4. Zia R, Schuller JA, Chandran A, Brongersma ML (2006) Plasmonics: the next chip-scale technology. Mater Today 9:20–27
5. Tao J, Wang QJ, Huang XG (2011) All-optical plasmonic switches based on coupled nano-disk cavity structures containing nonlinear material. Plasmonics 6:753–759
6. Veronis G, Fan S (2005) Bends and splitters in metal-dielectric-metal subwavelength plasmonic waveguides. Appl Phys Lett 87: 131102
7. Zhang Z, Shi FH, Chen YH (2015) Tunable multichannel plasmonic filter based on coupling-induced mode splitting. Plasmonics 10: 139–144
8. Fan CR, Shi FH, Wu HX, Chen YH (2015) Tunable all-optical plasmonic diode based on Fano resonance in nonlinear waveguide coupled with cavities. Opt Lett 40:2449–2452
9. Han ZH, Liu L, Forsberg E (2006) Ultra-compact directional couplers and Mach-Zehnder interferometers employing surface plasmon polaritons. Opt Commun 259:690–695
10. Wang B, Wang GP (2005) Plasmon Bragg reflectors and nanocavities on flat metallic surfaces. Appl Phys Lett 87:013107
11. Hu X, Li M, Ye Z, Leung WY, Ho KM, Lin SY (2008) Design of midinfrared photodetectors enhanced by resonant cavities with subwavelength metallic gratings. Appl Phys Lett 93:241108
12. Zhao F, Zhang C, Chang H, Hu X (2014) Design of plasmonic perfect absorbers for quantum-well infrared photodetection. Plasmonics 9:1397–1400
13. Zhang C, Chang H, Zhao F, Hu X (2013) Design principle of Au grating couplers for quantum-well infrared photodetectors. Opt Lett 38:4037–4039
14. Landy NI, Bingham CM, Tyler T, Jokerst N, Smith DR, Padilla WJ (2009) Design, theory, and measurement of a polarization-insensitive absorber for terahertz imaging. Phys Rev B 79:125104
15. Catchpole KR, Polman A (2008) Plasmonic solar cells. Opt Express 16:21793–21800
16. Diem M, Koschny T, Soukoulis CM (2009) Wide-angle perfect absorber/thermal emitter in the terahertz regime. Phys Rev B 79: 033101
17. García-Vidal FJ, Pitarke JM, Pendry JB (1997) Effective medium theory of the optical properties of aligned carbon nanotubes. Phys Rev Lett 78:4289–4292
18. Kravets VG, Neubeck S, Grigorenko AN (2010) Plasmonic blackbody: strong absorption of light by metal nanoparticles embedded in a dielectric matrix. Phys Rev B 81:165401
19. Grande M, Vincenti MA, Stomeo T, Bianco GV, Ceglia D, Aközbek N, Petruzzelli V, Bruno G, De Vittorio M, Scalora M, D'Orazio A (2014) Graphene-based absorber exploiting guided mode resonances in one-dimensional gratings. Opt Express 22: 31511–31519
20. Landy NI, Sajuyigbe S, Mock JJ, Smith DR, Padilla WJ (2008) Perfect metamaterial absorber. Phys Rev Lett 100:207402
21. Bouchon P, Koechlin C, Pardo F, Haïdar R, Pelouard JL (2012) Wideband omnidirectional infrared absorber with a patchwork of plasmonic nanoantennas. Opt Lett 37:1038–1040
22. Zhang BX, Zhao YH, Hao QZ, Kiraly B, Khoo IC, Chen SF, Huang TJ (2011) Polarization-independent dual-band infrared perfect absorber based on a metal-dielectric-metal elliptical nanodisk array. Opt Express 19:15221–15228
23. Collin S, Pardo F, Teissier R, Pelouard JL (2004) Efficient light absorption in metal-semiconductor-metal nanostructures. Appl Phys Lett 85:194–196
24. Malassis L, Massé P, Tréguer-Delapierre M, Mornet S, Weisbecker P, Barois P, Simovski CR, Kravets VG, Grigorenko AN (2014) Topological darkness in self-assembled plasmonic metamaterials. Adv Mater 26:324–330
25. Amin M, Farhat M, Bağcı H (2013) An ultra-broadband multilayered graphene absorber. Opt Express 21:29938–29948
26. Kaliteevski M, Iorsh I, Brand S, Abram RA, Chamberlain JMK, Kavokin AV, Shelykh IA (2007) Tamm plasmon-polaritons: possible electromagnetic states at the interface of a metal and a dielectric Bragg mirror. Phys Rev B 76:165415
27. Kavokin AV, Shelykh IA, Malpuech G (2005) Lossless interface modes at the boundary between two periodic dielectric structures. Phys Rev B 72:233102
28. Symonds C, Lheureux G, Hugonin JP, Greffet JJ, Laverdant J, Brucoli G, Lemaitre A, Senellart P, Bellessa J (2013) Confined Tamm plasmon lasers. Nano Lett 13:3179–3184
29. Zhang XL, Song JF, Li XB, Feng J, Sun HB (2012) Optical Tamm states enhanced broad-band absorption of organic solar cells. Appl Phys Lett 101:243901
30. Lee KJ, Wu JW, Kim K (2013) Enhanced nonlinear optical effects due to the excitation of optical Tamm plasmon polaritons in one-dimensional photonic crystal structures. Opt Express 21:28817–28823
31. Zhang WL, Yu SF (2010) Bistable switching using an optical Tamm cavity with a Kerr medium. Opt Commun 283:2622–2626
32. Zhang WL, Wang F, Rao YJ, Jiang Y (2014) Novel sensing concept based on optical Tamm plasmon. Opt Express 22:14524–14529
33. Fano U (1961) Effects of configuration interaction on intensities and phase shifts. Phys Rev 124:1866–1878
34. Kroner M, Govorov AO, Remi S, Biedermann B, Seidl S, Badolato A, Petroff PM, Zhang W, Barbour R, Gerardot BD, Warburton RJ, Karrai K (2008) The nonlinear Fano effect. Nature 451:311–314
35. Palik ED (1998) Handbook of optical constants of solids. Vol. I, II, and III. Academic press
36. Han ZH, Forsberg E, He SL (2007) Surface plasmon Bragg gratings formed in metal-insulator-metal waveguides. IEEE Photon Technol Lett 19:91–93
37. Dionne JA, Sweatlock LA, Atwater HA (2006) Plasmon slot waveguides: towards chip-scale propagation with subwavelength-scale localization. Phys Rev B 73:035407
38. Taflove A, Hagness SC (2000) Computational electrodynamics: the finite-difference time-domain method. Artech House Publishers, Boston
39. Bethune DS (1989) Optical harmonic generation and mixing in multilayer media: analysis using optical transfer matrix techniques. J Opt Soc Am B 6:910–916
40. Chen ZF, Han P, Leung CW, Wang Y, Hu MZ, Chen YH (2012) Study of optical Tamm states based on the phase properties of one-dimensional photonic crystals. Opt Express 20:21618–21626
41. Kang XB, Tan W, Wang ZG, Chen H (2009) Optic Tamm states: the Bloch-wave-expansion method. Phys Rev A 79:043832
42. Vinogradov AP, Dorofeenko AV, Erokhin SG, Inoue M, Lisyansky AA, Merzlikin AM, Granovsky AB (2006) Surface state peculiarities in one-dimensional photonic crystal interfaces. Phys Rev B 74: 045128
43. Boyd RW (2003) Nonlinear optics, 2nd ed. Academic press
44. Ricard D, Roussignol P, Flytzanis C (1985) Surface-mediated enhancement of optical phase conjugation in metal colloids. Opt Lett 10:511–513
45. Miroshnichenko AE, Flach S, Kivshar YS (2010) Fano resonances in nanoscale structures. Rev Mod Phys 82:2257–2298